Supplementary Information

Table of Contents

Detailed Description of Imaging Methods

Brain Imaging and Spectroscopy

All brain imaging and spectroscopy examinations were performed on a 3T Siemens MRI scanner (Biograph mMR, Siemens Healthineers, Erlangen, Germany) using a 16-channel phased array head (12-channels) and neck (4-channels) radiofrequency (RF) coil. A 60-minute brain MRI scan to acquire imaging and spectroscopy data was performed pre-HD and repeated during the last 60 minutes of dialysis.

Anatomical Brain Imaging

Whole-brain, three-dimensional T_1-weighted anatomical images were acquired using a magnetization-prepared rapid gradient-echo imaging sequence[1] with the following parameters: isotropic voxel resolution=1 mm^3, repetition time (TR)=2000 ms, echo-time (TE)=2.98 ms, inversion time=900 ms, acceleration factor=2, flip angle=9º. These images were used for volumetric analysis and for determining fractions of gray matter (GM), WM, and cerebrospinal fluid (CSF) needed during the calculation of diffusion metrics and metabolite concentrations.

Diffusion Tensor Imaging

Diffusion-weighted imaging (DWI) data for assessing brain WM structural integrity were acquired over 11 minutes using a single-shot echo-planar imaging (EPI) sequence with the following parameters: 2 mm isotropic resolution, 64 contiguous slices, b-values=0, 1000 s/mm^2 and 64 diffusion-encoding directions. To enable post-acquisition DWI correction for susceptibility-induced distortions, two spin-echo images were acquired in opposite phase-encoding directions with b-values=0 s/mm^2 and 6 repetitions.

Magnetic Resonance Spectroscopy

Single-voxel proton magnetic resonance spectroscopy (^{1}H-MRS) data were acquired using the semi-LASER (localization by adiabatic selective refocusing) sequence[2,3] in the CMRR Spectroscopy Package. The MRS package was developed by Gülin Öz and Dinesh Deelchand[3,4] and provided by the University of Minnesota under a C2P agreement. Water suppressed and unsuppressed ^{1}H-MRS data were collected from a 20×20×20 mm^3 voxel placed in the right prefrontal cortex WM (Supplementary Figure 1a) with the following parameters: TR=2000 ms, TE=67.60 ms, number of points=2048, bandwidth=2000 Hz, averages=128 for the water suppressed data, and averages=2 for the water unsuppressed data. The spectroscopy voxel was placed using anatomical landmarks visualized on the T_1-weighted anatomical images.

Image Processing and Analysis

Volumetric Analysis

Voxel-based morphometry (VBM) was performed on the T_1-weighted images. Simply put, this technique enabled the classification of voxels in the pre-HD and late-HD T_1-weighted images as GM, WM, or CSF. With the GM, WM, and CSF segmentations in hand, differences in GM, WM, and CSF volumes between pre-HD and late-HD as well as the spatial location of those differences could be estimated.

More specifically the longitudinal processing module (default option) in the Computational Anatomy Toolbox (CAT12, www.neuro.uni-jena.de/cat/) extension of the Statistical Parametric Mapping software (SPM12, www.fil.ion.ucl.ac.uk/spm/), optimized for detection of subtle changes over relatively short time intervals was used to preprocess, segment, and analyze images from pre-HD and late-HD in an unbiased manner. An inverse-consistent rigid-body registration approach was used for intra-subject alignment of each participant's pre-

HD and late-HD T_1-weighted images to one unbiased image space, which also included bias correction to minimize noise and intensity inhomogeneities. The bias-corrected and realigned images were first segmented into GM, WM, and CSF probability maps, then spatially normalized to the Montreal Neurological Institute (MNI) standard space using a non-linear DARTEL registration approach[5] and a mean deformation field estimated first for each timepoint, and finally averaged. The tissue segmentations were modulated by the Jacobian determinant of the mean deformation field to correct for non-linear differences in individual brain size and smoothed with an 8-mm full-width at half-maximum (FWHM) Gaussian kernel.

Analysis of Cerebral White Matter Integrity

To measure changes in brain WM microstructural integrity, the DWI images at pre-HD and late-HD were carefully preprocessed and analyzed to produce DTI scalar maps using an in-house image analysis pipeline implemented to incorporate steps from a variety of established image processing software packages as described previously.[6] Each participant's DWI images were denoised using an optimized non-local means filter in MATLAB (2018a, MathWorks®, Natick, MA),[7] then corrected for subject head motion, eddy currents, and signal intensity inhomogeneities using FMRIB's Software Library (FSL),[8] MRtrix3,[9] and Advanced Normalization Tools (ANTs),[10] respectively. A non-linear least-squares estimation approach in ExploreDTI[11] was used to fit tensors to DWI data and generate DTI scalar maps; fractional anisotropy (FA), mean diffusivity (MD), axial diffusivity (AD), and radial diffusivity (RD). The DTI scalar maps were spatially normalized to MNI space using a three-step registration algorithm, consisting of rigid, affine, and deformable transformations to a standard MNI T_1 1-mm template available in ANTs.

Quantification of Brain Metabolite Concentrations

Brain metabolite concentrations were calculated directly from the ^{1}H-MRS spectra as previously described.[12] The ^{1}H-MRS was first post-processed with QUALITY deconvolution and eddy current correction (QUECC),[13] with the number of QUALITY (quantification improvement by converting lineshapes to the Lorentzian type)[14] points chosen by fitting the water unsuppressed data in the time-domain with a decaying exponential function, determining the decay time constant, and choosing the number of points that corresponded to 2.5 times the decay time constant. Further post-processing of water-suppressed spectra involved removing residual water signal with a Hankel singular value decomposition algorithm. Then, using in-house software called fitMAN[15] and MAGIQ (www.github.com/dwong263/MAGIQ), water-suppressed spectra were fitted to simulated, 3T semi-LASER prior knowledge templates that included a predefined set of metabolites (Supplementary Table 1) and an empirically measured macromolecule model[16] (Supplementary Figure 1b), an approach previously described elsewhere.[17] Fitting was done using a Levenberg-Marquardt minimization algorithm[18] with pre-defined constraints (Supplementary Table 1). Metabolite concentrations were then calculated as previously described,[12,19] incorporating corrections for number of averages, gain and scaling factors applied to the data, the number of ^{1}H-MRS visible nuclei in water, the T_1 and T_2 relaxation rates of water in GM, WM, and CSF at 3T (Supplementary Table 2), and the partial volumes of GM, WM, and CSF in the spectroscopy voxel. Partial volumes needed for the concentration calculations were obtained from the T_1-weighted anatomical images using FSL software tools, version 5.0.10.[8,20,21]

Supplementary Results

Laboratory Testing

Linear mixed modeling revealed a significant effect of timepoint for potassium ($F(2,16) = 34.485$, $p = 0.000001$), phosphate ($F(2,16) = 29.604$, $p = 0.000003$), and magnesium ($F(2,16) = 10.760$, $p = 0.001$). Post-hoc testing showed a significant drop in potassium ($p < 0.001$), phosphate ($p < 0.001$), and magnesium ($p < 0.01$) from the start of dialysis to the last 60 minutes of dialysis, and to the end of dialysis (Supplementary Figure 2a). Tests for coagulation revealed a significant effect of timepoint for INR ($F(2,16) = 5.494$, $p = 0.015$) and PTT ($F(2,16) = 6.706$, $p = 0.008$). Post-hoc testing showed a significant increase in INR ($p = 0.038$) and PTT ($p = 0.015$) from the start of dialysis to the last 60 minutes of dialysis, and a significant decrease in INR ($p = 0.020$) and PTT ($p = 0.007$) from the last 60 minutes of dialysis to the end of dialysis (Supplementary Figure 2c).

For complete blood count, hemoglobin, white blood cell count, and platelet count were recorded. There were no significant changes from the start of dialysis to the end of dialysis for white blood cell and platelet counts. Linear mixed modeling did reveal a significant effect of timepoint for hemoglobin ($F(2,16) = 19.644$, $p = 0.00005$), with post-hoc testing showing a significant increase in hemoglobin from the start of dialysis to the last 60 minutes of dialysis ($p = 0.00015$) and to the end of dialysis ($p = 0.00014$, Supplementary Figure 2d).

Serum levels of bicarbonate, urea, lactate, and creatinine (Supplementary Figure 2b) showed a significant effect of timepoint for bicarbonate ($F(2.16) = 35.737$, $p = 0.000001$), urea ($F(2,16) = 89.180$, $p = 0.000000001$), and creatinine ($F(2,16) = 89.198$, $p = 0.0000000015$). Post-hoc testing showed the bicarbonate levels increased significantly from

the start of dialysis to the last 60 minutes of dialysis ($p = 0.0000007$) and to the end of dialysis ($p = 0.00003$). Urea and creatinine levels dropped significantly from the start of dialysis to the last 60 minutes of dialysis ($p < 0.001$) and to the end of dialysis ($p < 0.001$).

Supplementary Figures

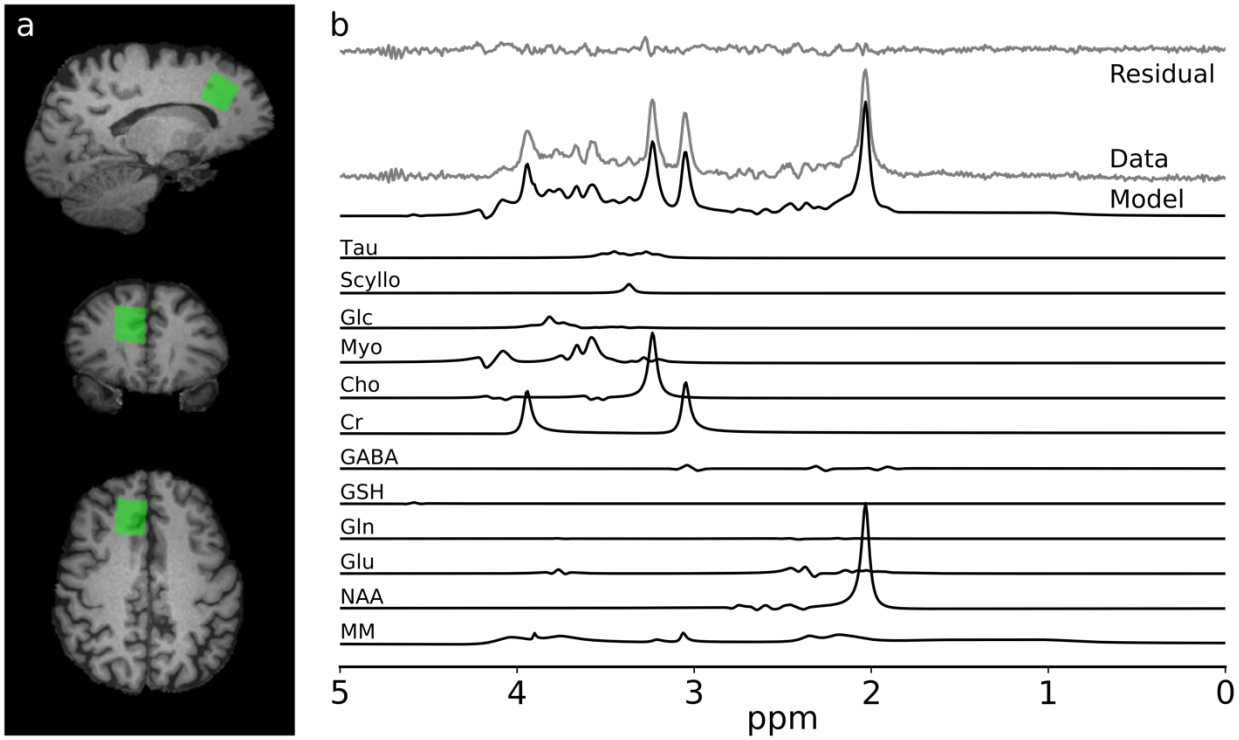

Supplementary Figure 1. A 20×20×20 mm³ spectroscopy voxel was placed in the right prefrontal cortex white matter according to anatomical landmarks. A representative example of voxel placement in one study participant is shown in (a). Spectroscopy data were fitted in the time-domain with simulated 3T semi-LASER prior knowledge templates that included an empirically measured macromolecule model. A representative spectrum from one study participant is shown in (b) with the fitted prior knowledge template ("Model"), the individual metabolite components, and the empirical macromolecule model ("MM").

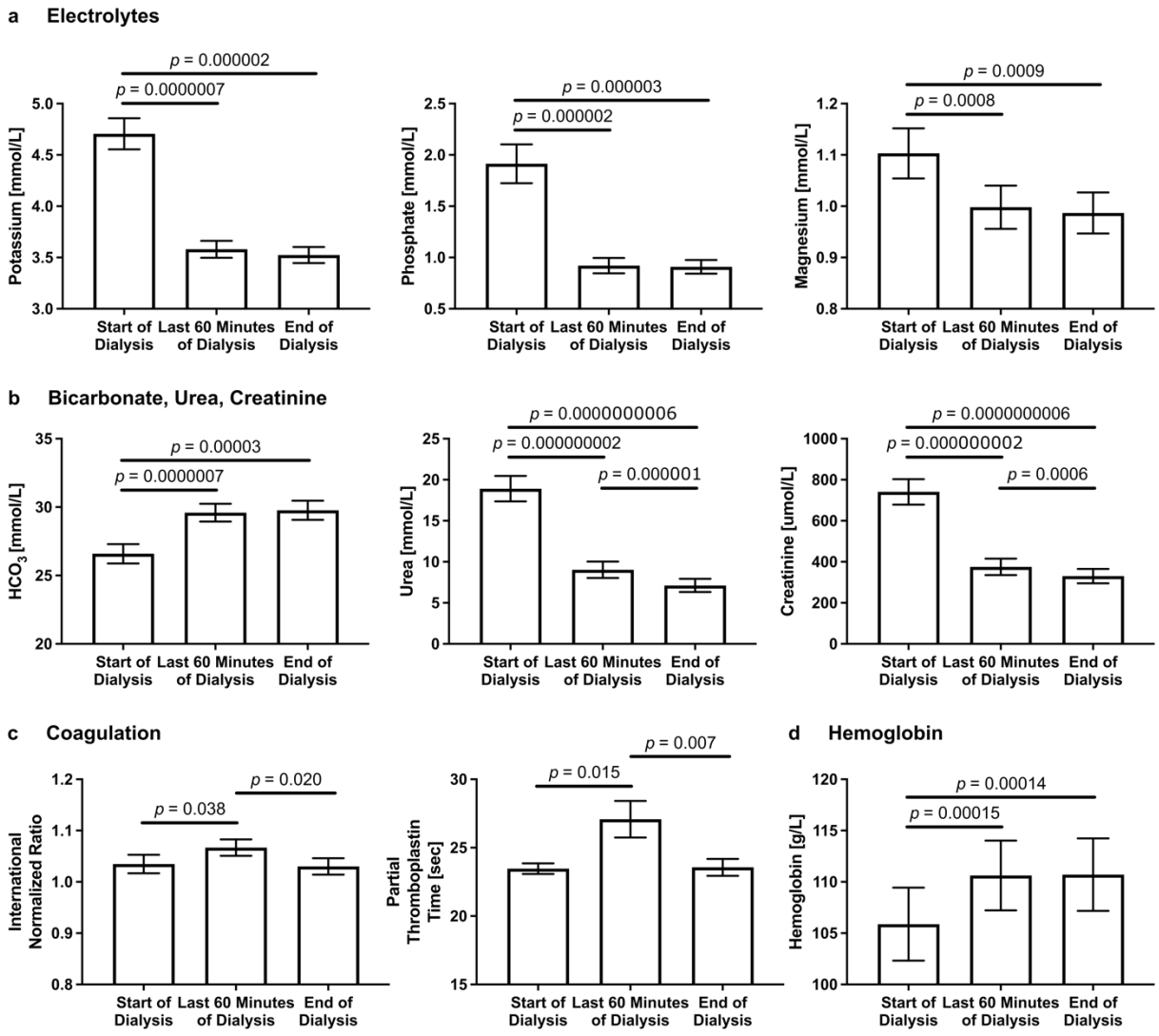

Supplementary Figure 2. Intradialytic changes in serum levels of electrolytes (potassium, magnesium, and phosphate) are shown in (a). Intradialytic changes in bicarbonate, urea, and creatine are shown in (b). Intradialytic changes international normalized ratio (INR), and partial thromboplastin (PTT) are shown in (c). Intradialytic changes hemoglobin levels are shown in (d). For all graphs, estimated marginal means and standard errors are plotted.

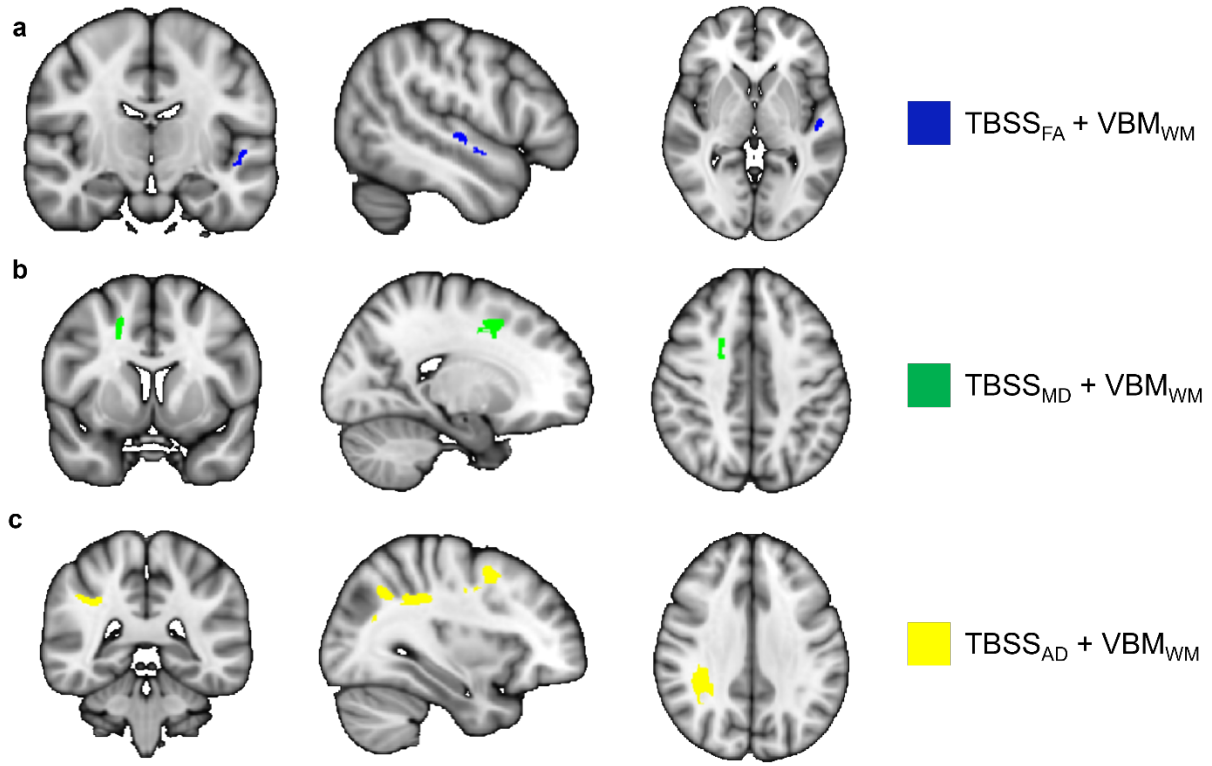

Supplementary Figure 3. White matter (WM) regions of concomitant intradialytic increase in WM volume from voxel-based morphometry (VBM) and increase in fractional anisotropy (FA, a) (MNI coordinates: Y=112, X=140, Z=72), increase in mean diffusivity (MD, b) (MNI coordinates: Y=133, X=70, Z=114), and increase in axial diffusivity (AD, c) (MNI coordinates: Y=87, X=57, Z=105) from tract-based spatial statistics (TBSS).

Supplementary Tables

Supplementary Table 1. A summary of relationships between metabolite parameters in the prior knowledge template[15]*. Peak positions (shifts) and phases of low-amplitude metabolites were linked to the shifts and phases of higher-amplitude metabolites. Within metabolites, peak amplitudes, shifts, and phases were fixed relative to one another. The following metabolites were included in the prior knowledge template: NAA, Glu, Gln, GSH, GABA, Cr, Cho, Myo, Glc, Scyllo, and Tau.*

Reference Metabolite	Linked Metabolites		Comments
	Shift	**Phase**	
NAA	Glu, Gln, GSH, GABA	Scyllo, Tau, Glc, GABA, Myo, Glu, Gln, GSH	• Shifts, phases, and amplitudes for Cr and Cho were not fixed relative to any reference metabolite. Cho and Cr were fitted independently. • A single linewidth parameter was defined for all metabolites. • A single delay time parameter was defined for all metabolites. • Parameters of the macromolecule model were not linked to parameters of any metabolites.
Myo	Glc, Scyllo, Tau		

Supplementary Table 2. A summary of the T_1 and T_2 values of metabolites and water in GM, WM, and CSF used for calculation of metabolite concentrations. All values were obtained from the literature as referenced in the table.

Metabolite	T_1 [s]			T_2 [s]		
	GM	**WM**	**Reference**	**GM**	**WM**	**Reference**
NAA	1.47	1.35	Mlynrik et. al55	247	295	Mlynrik et. al55
Glu	1.27	1.17		122	124	Wyss et al.56
Gln	1.23[a]	1.01[a]		99	168	
GSH	1.23[a]	1.01[a]		72	145	
GABA	1.23[a]	1.01[a]		75	161[a]	
Cre	1.46	1.24	Mlynrik et. al55	152	156	Mlynrik et. al 55
Cho	1.30	1.08		207	187	
Myo	1.23	1.01		229	161	Wyss et al.56
Glc	1.23[a]	1.01[a]		88	155	
Scy	1.23[a]	1.01[a]		107	170	
Tau	1.23[a]	1.01[a]		102	161[a]	
	T_1 [s]			**T_2 [s]**		
	GM	**WM**	**CSF**	**GM**	**WM**	**CSF**
Water	1.49525[b]	0.974577[b]	4.658333[b]	0.974577[b]	70[b]	503[c]

[a] T_1 and T_2 values of metabolites which were not available in the literature were assumed to be similar to that of Myo[24,25].
[b] T_1 values of water in GM, WM, and CSF were averaged from all reported values compiled in Bojorquez et al.59 Similarly, T_2 values of water in GM and WM were averaged from all reported values compiled in Bojorquez et al.[26]
[c] T_2 value of water in CSF was obtained from Piechnik et al.[27]

References

1. Brant-Zawadzki M, Gillan GD, Nitz WR: MP RAGE: A three-dimensional, T1-weighted, gradient-echo sequence - Initial experience in the brain. *Radiology* 182: 769–775, 1992
2. Garwood M, DelaBarre L: The return of the frequency sweep: designing adiabatic pulses for contemporary NMR. *Journal of Magnetic Resonance* [Internet] 153: 155–77, 2001 Available from: http://www.ncbi.nlm.nih.gov/pubmed/11740891
3. Oz G, Tkáč I: Short-echo, single-shot, full-intensity proton magnetic resonance spectroscopy for neurochemical profiling at 4 T: validation in the cerebellum and brainstem. *Magn Reson Med* [Internet] 65: 901–10, 2011 Available from: http://www.ncbi.nlm.nih.gov/pubmed/21413056
4. Deelchand DK, Berrington A, Noeske R, Joers JM, Arani A, Gillen J, et al.: Across-vendor standardization of semi-LASER for single-voxel MRS at 3T. *NMR Biomed* [Internet] 34: e4218, 2021 Available from: https://onlinelibrary.wiley.com/doi/full/10.1002/nbm.4218 [cited 2022 Jan 27]
5. Ashburner J: A fast diffeomorphic image registration algorithm. *Neuroimage* [Internet] 38: 95–113, 2007 Available from: www.elsevier.com/locate/ynimg [cited 2021 Dec 4]
6. Poirier SE, Kwan BYM, Jurkiewicz MT, Samargandy L, Steven DA, Suller-Marti A, et al.: 18F-FDG PET-guided diffusion tractography reveals white matter abnormalities around the epileptic focus in medically refractory epilepsy: implications for epilepsy surgical evaluation. *Eur J Hybrid Imaging* [Internet] 4: 2020 Available from: https://doi.org/10.1186/s41824-020-00079-7 [cited 2022 Jan 5]
7. Coupé P, Manjón J v., Gedamu E, Arnold D, Robles M, Collins DL: Robust Rician noise estimation for MR images. *Med Image Anal* 14: 483–493, 2010
8. Jenkinson M, Beckmann CF, Behrens TEJ, Woolrich MW, Smith SM: FSL. *Neuroimage* [Internet] 62: 782–790, 2012 Available from: https://www.sciencedirect.com/science/article/pii/S1053811911010603?via%3Dihub [cited 2018 Aug 25]
9. Tournier JD, Smith R, Raffelt D, Tabbara R, Dhollander T, Pietsch M, et al.: MRtrix3: A fast, flexible and open software framework for medical image processing and visualisation. Neuroimage. 202: 116137, 2019
10. Avants BB, Tustison NJ, Song G, Cook PA, Klein A, Gee JC: A reproducible evaluation of ANTs similarity metric performance in brain image registration. *Neuroimage* 54: 2033–2044, 2011
11. Leemans A, Jeurissen B, Sijbers J, Jones DK: ExploreDTI: a graphical toolbox for processing, analyzing, and visualizing diffusion MR data. 2009
12. Wong D, Atiya S, Fogarty J, Montero-Odasso M, Pasternak SH, Brymer C, et al.: Reduced Hippocampal Glutamate and Posterior Cingulate N-Acetyl Aspartate in Mild Cognitive Impairment and Alzheimer's Disease Is Associated with Episodic Memory Performance and White Matter Integrity in the Cingulum: A Pilot Study. *Journal of Alzheimer's Disease* [Internet] Preprint: 1–21, 2020 Available from: https://www.medra.org/servlet/aliasResolver?alias=iospress&doi=10.3233/JAD-190773 [cited 2020 Feb 10]
13. Bartha R, Drost DJ, Menon RS, Williamson PC: Spectroscopic lineshape correction by QUECC: combined QUALITY deconvolution and eddy current correction. *Magn Reson Med* [Internet] 44: 641–5, 2000 Available from: http://doi.wiley.com/10.1002/1522-

2594%28200010%2944%3A4%3C641%3A%3AAID-MRM19%3E3.0.CO%3B2-G [cited 2016 Mar 9]
14. de Graaf AA, van Dijk JE, BoéE WMMJ: QUALITY: quantification improvement by converting lineshapes to the lorentzian type. *Magn Reson Med* [Internet] 13: 343–357, 1990 Available from: http://doi.wiley.com/10.1002/mrm.1910130302 [cited 2016 Mar 9]
15. Bartha R, Drost DJ, Williamson PC: Factors affecting the quantification of short echo in-vivo 1H MR spectra: prior knowledge, peak elimination, and filtering. *NMR Biomed* [Internet] 12: 205–16, 1999 Available from: http://doi.wiley.com/10.1002/%28SICI%291099-1492%28199906%2912%3A4%3C205%3A%3AAID-NBM558%3E3.0.CO%3B2-1 [cited 2016 Nov 7]
16. Birch R, Peet AC, Dehghani H, Wilson M: Influence of macromolecule baseline on 1H MR spectroscopic imaging reproducibility. *Magn Reson Med* 77: 34–43, 2017
17. Wong D, Schranz AL, Bartha R: Optimized in vivo brain glutamate measurement using long-echo-time semi-LASER at 7 T. *NMR Biomed* [Internet] 31: e4002, 2018 Available from: http://doi.wiley.com/10.1002/nbm.4002 [cited 2018 Aug 24]
18. Marquardt DW: An Algorithm for Least-Squares Estimation of Nonlinear Parameters. *Journal of the Society for Industrial and Applied Mathematics* [Internet] 11: 431–441, 1963 Available from: http://epubs.siam.org/doi/10.1137/0111030 [cited 2017 May 14]
19. Gasparovic C, Song T, Devier D, Bockholt HJ, Caprihan A, Mullins PG, et al.: Use of tissue water as a concentration reference for proton spectroscopic imaging. *Magn Reson Med* [Internet] 55: 1219–1226, 2006 Available from: http://doi.wiley.com/10.1002/mrm.20901 [cited 2018 Nov 13]
20. Smith SM, Jenkinson M, Woolrich MW, Beckmann CF, Behrens TEJ, Johansen-Berg H, et al.: Advances in functional and structural MR image analysis and implementation as FSL. *Neuroimage* [Internet] 23: S208–S219, 2004 Available from: https://www.sciencedirect.com/science/article/pii/S1053811904003933?via%3Dihub [cited 2018 Aug 25]
21. Woolrich MW, Jbabdi S, Patenaude B, Chappell M, Makni S, Behrens T, et al.: Bayesian analysis of neuroimaging data in FSL. *Neuroimage* [Internet] 45: S173–S186, 2009 Available from: https://www.sciencedirect.com/science/article/pii/S1053811908012044?via%3Dihub [cited 2018 Aug 25]
22. Mlynrik V, Gruber S, Moser E: Proton T1 and T2 relaxation times of human brain metabolites at 3 Tesla. *NMR Biomed* [Internet] 14: 325–331, 2001 Available from: http://doi.wiley.com/10.1002/nbm.713 [cited 2019 Nov 3]
23. Wyss PO, Bianchini C, Scheidegger M, Giapitzakis IA, Hock A, Fuchs A, et al.: In vivo estimation of transverse relaxation time constant (T2) of 17 human brain metabolites at 3T. *Magn Reson Med* [Internet] 80: 452–461, 2018 Available from: http://doi.wiley.com/10.1002/mrm.27067 [cited 2019 Nov 3]
24. Marjańska M, Auerbach EJ, Valabrègue R, van de Moortele P-F, Adriany G, Garwood M: Localized 1H NMR spectroscopy in different regions of human brain in vivo at 7 T: T2 relaxation times and concentrations of cerebral metabolites. *NMR Biomed* [Internet] 25: 332–339, 2012 Available from: http://doi.wiley.com/10.1002/nbm.1754 [cited 2015 Aug 26]

25. Kreis R, Slotboom J, Hofmann L, Boesch C: Integrated data acquisition and processing to determine metabolite contents, relaxation times, and macromolecule baseline in single examinations of individual subjects. *Magn Reson Med* [Internet] 54: 761–768, 2005 Available from: http://doi.wiley.com/10.1002/mrm.20673 [cited 2016 Nov 7]
26. Bojorquez JZ, Bricq S, Acquitter C, Brunotte F, Walker PM, Lalande A: What are normal relaxation times of tissues at 3 T? Magn Reson Imaging. 35: 69–80, 2017
27. Piechnik SK, Evans J, Bary LH, Wise RG, Jezzard P: Functional changes in CSF volume estimated using measurement of water T2 relaxation. *Magn Reson Med* [Internet] 61: 579–586, 2009 Available from: https://onlinelibrary.wiley.com/doi/full/10.1002/mrm.21897 [cited 2021 Aug 26]